



Colloid Transport of Plutonium in the Far-Field of the Mayak Production Association, Russia

Alexander P. Novikov, *et al.*

Science **314**, 638 (2006);

DOI: 10.1126/science.1131307

The following resources related to this article are available online at www.sciencemag.org (this information is current as of November 3, 2008):

Updated information and services, including high-resolution figures, can be found in the online version of this article at:

<http://www.sciencemag.org/cgi/content/full/314/5799/638>

Supporting Online Material can be found at:

<http://www.sciencemag.org/cgi/content/full/314/5799/638/DC1>

This article has been **cited by** 15 article(s) on the ISI Web of Science.

This article has been **cited by** 2 articles hosted by HighWire Press; see:

<http://www.sciencemag.org/cgi/content/full/314/5799/638#otherarticles>

This article appears in the following **subject collections**:

Geochemistry, Geophysics

http://www.sciencemag.org/cgi/collection/geochem_phys

Information about obtaining **reprints** of this article or about obtaining **permission to reproduce this article** in whole or in part can be found at:

<http://www.sciencemag.org/about/permissions.dtl>

energies of 9.687, 9.886, 14.414, and 33.678 keV. The x-ray-induced reaction in ice VII was most effective with 9.687- and 9.886-keV x-radiation, which are absorbed readily by H₂O; was less effective with 14.414-keV x-radiation; and was not observed with 33.678-keV high-energy x-radiation, which passed through H₂O without adequate absorption. High-pressure synchrotron XRD studies typically use high-energy x-radiation above 20 keV with short exposure times of seconds to minutes; this would be insufficient to induce the reaction. On the other hand, low-energy x-radiation below 12 keV would be largely absorbed by the diamond anvils and are seldom used for XRD studies. In our experiments, the ~10-keV x-rays pass through the low-absorbance Be gasket and provide optimal conditions for inducing the reaction.

References and Notes

- V. F. Petrenko, R. W. Whitworth, *Physics of Ice* (Oxford Univ. Press, New York, 1999).
- I.-M. Chou *et al.*, *Science* **281**, 809 (1998).
- C. Lobban, J. L. Finney, W. F. Kuhs, *Nature* **391**, 268 (1998).
- J. S. Tse, D. D. Klug, *Phys. Rev. Lett.* **81**, 2466 (1998).
- Y. Q. Cai *et al.*, *Phys. Rev. Lett.* **94**, 025502 (2005).
- O. Mishima, L. D. Calvert, E. Whalley, *Nature* **310**, 393 (1984).
- R. J. Hemley, L. C. Chen, H. K. Mao, *Nature* **338**, 638 (1989).
- J. L. Finney *et al.*, *Phys. Rev. Lett.* **88**, 225503 (2002).
- C. A. Tulk *et al.*, *Science* **297**, 1320 (2002).
- A. F. Goncharov, V. V. Struzhkin, M. S. Somayazulu, R. J. Hemley, H. K. Mao, *Science* **273**, 218 (1996).
- M. Bernasconi, P. L. Silvestrelli, M. Parrinello, *Phys. Rev. Lett.* **81**, 1235 (1998).
- A. F. Goncharov, V. V. Struzhkin, H. K. Mao, R. J. Hemley, *Phys. Rev. Lett.* **83**, 1998 (1999).
- C. Cavazzoni *et al.*, *Science* **283**, 44 (1999).
- A. F. Goncharov *et al.*, *Phys. Rev. Lett.* **94**, 125508 (2005).
- O. Mishima, H. E. Stanley, *Nature* **396**, 329 (1998).
- L. Liu *et al.*, *Phys. Rev. Lett.* **95**, 117802 (2005).
- W. L. Mao *et al.*, *Science* **302**, 425 (2003).
- Y. Meng *et al.*, *Nat. Mater.* **3**, 111 (2004).
- S. K. Lee *et al.*, *Nat. Mater.* **4**, 851 (2005).
- S. K. Sharma, H. K. Mao, P. M. Bell, *Phys. Rev. Lett.* **44**, 886 (1980).
- Y. A. Freiman, H. J. Jodl, *Phys. Rep.* **401**, 1 (2004).
- Y. Akahama, H. Kawamura, *Phys. Rev. B* **54**, R15602 (1996).
- P. Loubeyre, R. Letoullec, J. P. Pinceaux, *Phys. Rev. Lett.* **67**, 3271 (1991).
- D. M. Brown, W. B. Daniels, *Phys. Rev. A* **45**, 6429 (1992).
- H. Fujihisa *et al.*, *Phys. Rev. Lett.* **97**, 085503 (2006).
- Y. Akahama *et al.*, *Phys. Rev. Lett.* **74**, 4690 (1995).
- G. Weck, P. Loubeyre, R. Letoullec, *Phys. Rev. Lett.* **88**, 035504 (2002).
- J.-F. Lin *et al.*, *Geophys. Res. Lett.* **32**, L11306 (2005).
- H. Cynn, C. S. Yoo, S. A. Sheffield, *J. Chem. Phys.* **110**, 6836 (1999).
- P. Loubeyre, R. Letoullec, *Nature* **378**, 44 (1995).
- Y. Fei, H. K. Mao, R. J. Hemley, *J. Chem. Phys.* **99**, 5369 (1993).
- We thank S. Ghosh for assistance with the XRS at APS; N. Hiraoka, I. Jarrige, H. Ishii, and C. C. Chen for assistance with the XRS at SPring-8; S. Sinogeiken for assistance with the ORS; and M. Somayazulu and A. Levedahl for assistance with resistive heating measurements. The NSF–Division of Materials Research (DMR-0508988), NSF–Division of Earth Sciences (EAR) Petrology and Geochemistry, NSF-EAR Geophysics, and NSF-EAR Instrumentation and Facility Programs provided financial support, and HPCAT provided synchrotron beam time. GeoSoilEnviro Consortium for Advanced Radiation Sources is supported by the NSF-EAR (EAR-0217473), U.S. Department of Energy (DOE)–Geosciences (DE-FG02-94ER14466), and State of Illinois. HPCAT is supported by the DOE–Basic Energy Sciences (BES), DOE–National Nuclear Security Administration, Carnegie DOE Alliance Center, NSF, Department of Defense–Tank-Automotive and Armaments Command, and W. M. Keck Foundation. APS is supported by the DOE-BSE, Office of Energy Research, under contract W-31-109-Eng-38. The work performed at BL12XU, SPring-8, is partly supported by the National Synchrotron Radiation Research Center and National Science Center of Taiwan.

21 July 2006; accepted 14 September 2006
10.1126/science.1132884

Colloid Transport of Plutonium in the Far-Field of the Mayak Production Association, Russia

Alexander P. Novikov,¹ Stepan N. Kalmykov,^{1,2} Satoshi Utsunomiya,³ Rodney C. Ewing,^{3*} François Horreard,⁴ Alex Merkulov,⁴ Sue B. Clark,⁵ Vladimir V. Tkachev,¹ Boris F. Myasoedov¹

Sorption of actinides, particularly plutonium, onto submicrometer-sized colloids increases their mobility, but these plutonium colloids are difficult to detect in the far-field. We identified actinides on colloids in the groundwater from the Mayak Production Association, Urals, Russia; at the source, the plutonium activity is ~1000 becquerels per liter. Plutonium activities are still 0.16 becquerels per liter at a distance of 3 kilometers, where 70 to 90 mole percent of the plutonium is sorbed onto colloids, confirming that colloids are responsible for the long-distance transport of plutonium. Nano-secondary ion mass spectrometry elemental maps reveal that amorphous iron oxide colloids adsorb Pu(IV) hydroxides or carbonates along with uranium carbonates.

Submicrometer-sized colloids, consisting of inorganic and/or organic compounds, occur at up to 10¹⁷ particles per liter in groundwater and provide an important means of trans-

porting elements with low solubilities, including the actinides (1–3). The stability of these colloids is a function of the composition of groundwater and the hydrologic conditions (4).

The formation of actinide pseudo-colloids, in which the actinide sorbs onto aquatic colloids, can stabilize actinides in natural waters and increase their concentrations by many orders of magnitude over the values expected from solubility calculations (2, 5). The association of Pu with colloids 25 to 450 nm in size has been observed 3.4 km from a source at Los Alamos National Laboratory (6). This migration distance is greater than modeled estimates (7). Similar transport has also been seen at the

Savannah River Site (8). At Nevada Test Site, Pu has migrated 1.3 km in 30 years in groundwater by means of colloids with sizes of 7 nm to 1 μm (9). Model results imply that colloid-facilitated transport of actinides at Yucca Mountain could lead to as much as a 60-fold increase in the total effective dose equivalent to an exposed population (10).

Colloid-facilitated transport is likely the means for actinides' long-distance transport in groundwater. Many previous studies have experimentally demonstrated adsorption of Pu onto a variety of minerals and mineral assemblage (11–13). However, little is known of the speciation of the actinides or the type of colloids with which they are associated, particularly during the transport in the far-field where there are many competing processes, such as desorption from the colloids and resorption onto minerals.

To understand the colloid-associated actinides and their long-distance transport in groundwater, we investigated Pu migration in the natural groundwater system at one of the most contaminated nuclear sites in the world: Mayak, Russia. Mayak is a nuclear waste reprocessing plant near Kyshtym, in the Southern Urals, Russia (14) (Fig. 1). Waste effluents containing ⁹⁰Sr, ¹³⁷Cs, ²⁴¹Am, and ²³⁹Pu were discharged into Lake Karachai (15, 16); these were weakly alkaline NaNO₃ brine solutions with a pH of 7.9 to 9.3 and a salt concentration of 16 to 145 g/liter. The major dissolved ionic species were NO₃⁻ (11 to 78 g/liter), CH₃COO⁻ (0.6 to 20 g/liter), C₂O₄²⁻ (0.9 to 14 g/liter), SO₄²⁻ (0.12 to 1.3 g/liter), Na⁺ (6 to 32 g/liter), Cl⁻ (20 to 350 mg/liter), U(VI) (13 to 196 mg/liter), Ca²⁺ (8 to 80 mg/liter), and

¹Vernadsky Institute of Geochemistry and Analytical Chemistry, Russian Academy of Sciences, Moscow 119991, Russia.

²Radiochemistry Division, Chemistry Department, Lomonosov Moscow State University, Moscow 119992, Russia. ³Department of Geological Sciences, University of Michigan, Ann Arbor, MI 48109–1005, USA. ⁴Cameca, 92622 Gennevilliers Cedex, 92403, France. ⁵Department of Chemistry and Nuclear Radiation Center, Washington State University, Pullman, WA 99164–4630, USA.

*To whom correspondence should be addressed. E-mail: rodewing@umich.edu

Mg²⁺ (8 to 69 mg/liter) (17). Lake Karachai is connected to the 55- to 100-m-thick groundwater zone, in which fluids flow through fractured Silurian and Devonian metavolcanic rocks with andesitic and basaltic composition (17). We completed systematic analyses of the composition and redox state of groundwaters and filtered samples, and we characterized the actinides associated with the colloids (18).

Because of the high concentration of NO₃⁻ in waste effluents, we used the presence of NO₃⁻ as a measure of the extent to which the contaminant plume had penetrated the groundwater system. The Pu radioactivity was ~4.8 becquerels (Bq)/liter at 0.05 km from the source, whereas it was ~0.029 Bq/liter at 4.0 km (Table 1), which is approximately equivalent to ~2.1 parts per trillion (ppt) and ~0.013 ppt, respectively, versus ~1000 Bq/liter (19) in the waste effluent. The redox potential, *E_h*, of the groundwater was +50 to ~+480 mV, and the pH was ~6 to 8. Nitrate concentrations decreased as distance from the source increased, although at greater depths (~100 m) original waste effluents with a relatively high concentration of Pu (0.16 Bq/liter) were present even 3.9 km from the source.

To understand stable chemical species of the actinides under the groundwater conditions, we constructed predominance diagrams for U and Pu species using thermodynamic calculation (20) with updated solubility data (21), based on the total concentrations of the groundwaters from the wells nearest to the source (Fig. 2, A and B) and from a well located 3.2 km away [well number 1, drilled in 1969 (1/69)] (Fig. 2, C and D). This analysis implies that UO₂(CO₃)₂²⁻ is the dominant species near the source, whereas UO₂(CO₃)₃⁴⁻ is present at well 1/69. However, the data (circles in Fig. 2, A and C) are close to the equilibrium

boundary between these two U carbonate species. Thus, it is likely that both of these U(VI) carbonate species are dominant in the groundwater of Mayak, which is consistent with the oxidation state analysis (table S1). In addition, the U distribution on the colloidal matter for fractions of different sizes also indicates that 80 to 90% of the U is present as a soluble species (Fig. 2E). Similarly, most of the Np (70 to 80%) is present as a soluble Np(V) phase (Fig. 2E and table S1), most likely as NpO₂⁺, as anticipated from the stability diagram (fig. S1).

The stability diagrams (Fig. 2, B and D) show that the total groundwater compositions near the source (solid square) and at the well 1/69 (open square) are in the region of solid PuO₂. Even though the solution is supersaturated with respect to crystalline plutonium

dioxide PuO_{2(c)}, the precipitation will require aging in order to dehydrate the metastable Pu hydroxyl species into PuO_{2(c)} (21, 22). Given that amorphous Pu(OH)₄ always precipitates from solution instead of PuO₂ (21), the stability field of amorphous plutonium hydroxide Pu(OH)_{4(am)} is also shown. The size dependence of the Pu distribution (Fig. 2E) shows that ~30 and ~10% of Pu is present as a soluble species in well 63/68 (near the source) and 1/69, respectively, which indicates that the actual Pu concentration in the “solution” was lower than the total Pu concentration in the groundwater. Because particles smaller than ~1 nm (the size of the 3-kD filter) were counted as a soluble species, a part of the Pu associated with the colloids, which are <1 nm, may have been counted as part of the soluble fraction. The

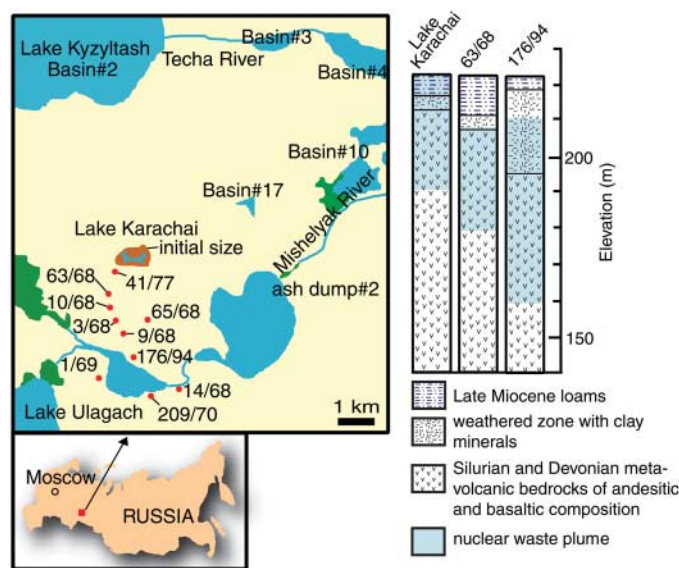


Fig. 1. Map of the study area. The locality map and stratigraphy are modifications of those in (17). The Mayak site covers ~160 km² (17). Red points labeled with the numbers are wells. The numbered basins are natural or man-made reservoirs for nuclear waste fluids.

Table 1. Concentration of actinides in the groundwaters from the Mayak region, Russia. The well index represents the well number followed by the drilling year (e.g., 41/77 is well 47, drilled in 1977). I.C., concentration of total inorganic carbon species in solution; n.d., not determined.

| Well index | Distance (km) | Depth (m) | <i>E_h</i> (mV) | pH | I.C. (ppm) | NO ₃ ⁻ (ppm) | ^{239,240} Pu (Bq/liter) | ²⁴¹ Am (Bq/liter) | ²³⁷ Np (Bq/liter) | ²³⁸ U (ppm) |
|------------|---------------|-----------|---------------------------|------|------------|------------------------------------|----------------------------------|------------------------------|------------------------------|------------------------|
| Source | 0.0 | | | | | <78,000 | 1,000 | 420 | 41 | 25 |
| 41/77 | 0.05 | 20 | +480 | 5.9 | 4,760 | 45,000 | 4.8 | 0.91 | 0.14 | n.d. |
| | | 45 | +50 | 8.05 | n.d. | n.d. | 2.8 | 0.34 | 0.12 | n.d. |
| 63/68 | 1.1 | 20 | +400 | 6.0 | 1,220 | 45,000 | 0.13 | 0.21 | 18.2 | 20 |
| | | 100 | +60 | 7.33 | n.d. | n.d. | 0.31 | 1.32 | 11.1 | 38 |
| 10/68 | 1.5 | 60 | +390 | 6.6 | 1,830 | 52,000 | 0.86 | 4.75 | 9.1 | 24 |
| | | 100 | +330 | 6.6 | n.d. | n.d. | 0.18 | 0.50 | 17.0 | 47 |
| 65/68 | 1.75 | 60 | +300 | 7.5 | n.d. | 28,000 | 0.46 | 0.72 | 2.8 | 0.3 |
| | | 100 | +200 | 6.9 | n.d. | n.d. | 0.052 | 0.094 | 2.2 | 1.1 |
| 3/68 | 1.9 | 60 | +350 | 7.1 | 1,160 | 32,000 | 1.62 | 0.29 | 10.4 | 38 |
| | | 100 | +300 | 6.45 | n.d. | n.d. | 1.19 | 0.40 | 12.2 | 43 |
| 9/68 | 2.15 | 60 | +310 | 7.60 | 952 | 27,100 | 0.036 | 1.10 | 5.8 | 26 |
| | | 100 | +350 | 5.85 | n.d. | n.d. | 0.21 | 1.08 | 10.9 | 36 |
| 176/94 | 2.5 | 27 | n.d. | n.d. | n.d. | n.d. | 3.0 | 0.7 | 0.36 | 3.2 |
| | | 63 | +90 | 7.33 | 251 | 3,910 | 0.8 | 0.11 | 0.78 | 2.8 |
| 1/69 | 3.2 | 44 | +100 | 7.9 | 159 | 21 | 0.089 | 0.15 | 2.1 | 0.26 |
| 14/68 | 3.9 | 100 | +100 | 7.9 | 200 | 498 | 0.16 | 0.087 | 2.5 | 19 |
| 209/70 | 4.0 | 40 | +50 | 8.12 | 136 | 6.5 | 0.029 | 0.08 | 0.03 | 0.02 |

actual Pu concentration in the groundwater could have been even lower than the percentage shown in Fig. 2E. Thus, the data points for the actual soluble Pu concentrations should be plotted at lower values in the diagram of Fig. 2, B and D, as indicated by the arrows. In the event that an intrinsic Pu(IV) phase precipitates from solution, the Pu concentrations in solution (data points in Fig. 2, B and D) will also be shifted downward to the stability field of aqueous plutonium hydroxide $\text{Pu}(\text{OH})_{4(\text{aq})}$ (the dashed arrows).

A dominant fraction of $\text{Pu}(\text{OH})_{4(\text{aq})}$ is not inconsistent with the oxidation state analysis that reveals a predominance of Pu(IV), although it is also possible that different chemical Pu(IV) species are incorporated into aquatic colloids. In addition, 70 to 90% of Pu was associated with the colloidal fraction on 3- and 10-kD filters (the size range of 1 to 15 nm). The ratio of Pu associated with colloids to soluble species (Fig. 2F) was nearly constant (~2.2) within 2.15 km of the source, regardless of the Pu concentration, and the values became higher (>5) at distances of >2.5 km (Fig. 2F) as well as U partitioning (Fig. 2G). This result suggests that Pu was partitioned between colloids and soluble species within 2.5 km, whereas at >2.5 km, the excess fraction of Pu-bearing colloids is transported in the groundwater system, ascribed to a disequilibrium derived from the slow desorption of Pu from the colloids or to the irreversible incorporation of trace Pu into aquatic colloids.

Electron microscopy analysis of the colloid fraction from well 1/69 revealed a variety of phases (Fig. 3A). Spherical Fe oxide and Fe hydroxide are the most abundant phases, and they are associated with minor Si and Ca that range in size from a few nanometers to 100 nm across, forming aggregates up to several micrometers in size (Fig. 3, B and C). Based on the electron diffraction pattern, the Fe oxide/hydroxide is characterized to be an amorphous Fe hydroxide (HFO). Amorphous HFO commonly occurs in soils and is known to be an efficient adsorbent of toxic metals (23). The other identified phases include clays and calcite; rutile, hematite, barite, and rancieite; and monazite, in decreasing order of abundance. Nano-secondary ion mass spectrometry (SIMS) elemental maps for the colloids from well 1/69 reveal that some Al and Mn are also associated with the Fe (Fig. 3D). The approximate atomic ratios of Al to Fe and Mn to Fe are ~0.003 and ~0.004, respectively. The amount of associated Ca is not less than the amount of Al and Mn but is at the same level as in the mixture of HFO (Fig. 3C). Thus, this aggregate of colloids can be characterized as amorphous HFO adsorbing less than 1 atomic % of Al and Mn.

The Pu map (Fig. 3D) is nearly the same as that of the U, which is associated with the Fe oxide. Semiquantitatively, the atomic ratio of U to Fe is ~0.0004, and the ratio of Pu to U is ~0.03, indicating that amorphous HFO is a pseudo-colloid sorbing both the Pu and U. Based

on the thermodynamic calculations for the expected, dominant Pu and U species, $\text{Pu}(\text{OH})_{4(\text{aq})}$ occurs with $\text{UO}_2(\text{CO}_3)_3^{4-}$ and to a lesser extent with $\text{UO}_2(\text{CO}_3)_2^{2-}$, subsequently sorbing onto the amorphous HFO. Because the SIMS analysis causes the destruction of the sample, there are no crystallographic data available for the same HFO grain for which Pu was detected by nano-SIMS and examined by electron microscopy. Elemental mapping of the other colloidal material showed that U is predominantly adsorbed onto amorphous HFO and to a lesser extent onto rancieite $[(\text{Ca},\text{Mn})\text{Mn}_4\text{O}_9\text{3H}_2\text{O}]$ and hematite (Fe_2O_3) (fig. S2). We did not find any intrinsic Pu(IV) colloids nor any actinide adsorption onto the other colloidal phases, including clays, calcite, rutile, barite, and monazite in the sample from well 1/69. These results are consistent with experiments that have reported a higher adsorption coefficient for Pu onto Fe oxide colloids than onto montmorillonite and silica (24). Additionally, the high ionic strength of this system may inhibit adsorption onto inorganic colloids, with the exception of Fe oxide (24). At distances greater than 2.5 km, the desorption process is anticipated to occur slowly, because the previous experiments revealed that the Pu desorption process from a hematite surface is considerably slower than the adsorption rate (24). Based on the Pu adsorption onto amorphous HFO in this system, most Pu(IV) in our oxidation analysis (table S1) may be the result of reduction of Pu(V) to Pu(IV) after adsorption

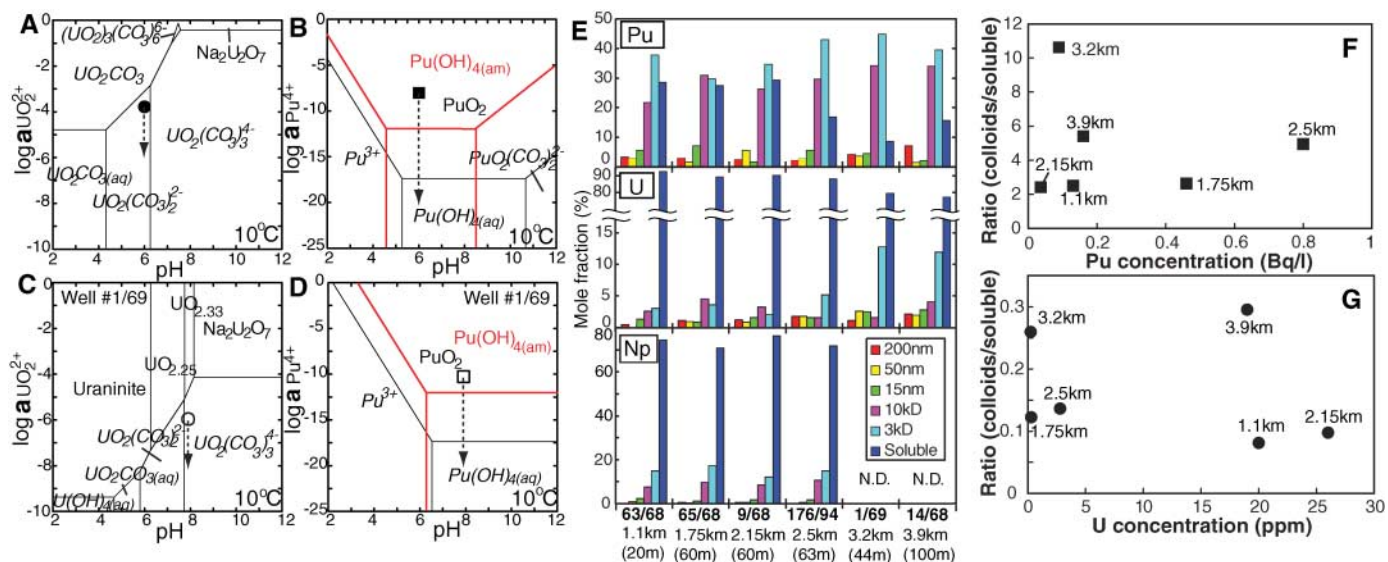


Fig. 2. Stable species of actinides and evidence of actinides bound to colloids. (A and B) Thermodynamic stability diagrams of U and Pu species under the conditions near Karachai Lake (well 41/77). (C and D) Thermodynamic stability diagram of U and Pu species under the conditions at well 1/69 located 3.9 km from the source at a depth of 44 m. Total concentrations in the groundwater are plotted as circles (U) and squares (Pu). Solid symbols show data near the source [(A) and (B)], and open symbols show the data at well 1/69 [(C) and (D)]. Roman and italic fonts represent solid and aqueous species, respectively. The arrows indicate the transition of solution composition that occurs when Pu precipitates as intrinsic or aquatic colloids or is sorbed onto pseudo-colloids. For these

thermodynamic calculations, Act-2 application (20) was used with the database of thermoco.com.v8.r6+, which is an expanded version of the Lawrence Livermore National Laboratory database. Solubility data of $\text{Pu}(\text{OH})_{4(\text{aq})}$ are updated based on (21). In illustrating the stability fields (red) of $\text{Pu}(\text{OH})_{4(\text{am})}$ in (B) and (D), the temperature was set to 25°C because of the limited solubility data in (21). (E) Mole fraction of actinides (Pu, U, and Np) bound to colloids as a function of the size. The 10- and 3-kD measures correspond to approximately 1.5 and 1.0 nm, respectively. N.D., not determined. (F and G) Ratios between actinides bound to colloids and in a soluble form for Pu and U. Pu and U concentrations are a total in the groundwaters. ppm, parts per million.

onto Fe oxide (11, 12). In addition, the high concentration of dissolved organic carbon (<20 g/liter of CH_3COO^-) near the source may result in the reduction of Pu(V) into Pu(IV) in solution, as reported in (12, 22). Even inorganic colloids can be coated by humic acid, forming pseudo-colloids, which can sorb the hydrolyzed species more strongly than simple inorganic colloids (22).

As compared with other minerals that may sorb actinides, the Fe oxides have a high zero point of charge (ZPC): 6.5 for Fe_3O_4 and 7.8 for $\alpha\text{-FeOOH}$ versus 4.6 for kaolinite, 2.5 for montmorillonite, 2 to 2.4 for feldspars, and 2.0 for SiO_2 (25). In particular, the ZPC for amorphous $\text{Fe}(\text{OH})_3$ is 8.5 (25), and the value should be the most appropriate for the HFO we found because of the amorphous structure of the Fe oxide/hydroxide. The high ZPC must result in the positive charge on the surface of HFO under the conditions in the Mayak groundwaters; thus, the particles should be efficient adsorbents of negatively charged U species. Although it is not evident how $\text{Pu}(\text{OH})_{4(\text{aq})}$ is adsorbed onto the HFO together with $\text{UO}_2(\text{CO}_3)_3^{4-}$, the hydroxyls of $\text{Pu}(\text{OH})_{4(\text{aq})}$ may be attached directly to the positively charged HFO surface. According to recent modeling studies (26), a Pu(IV) carbonate species, $\text{Pu}(\text{CO}_3)_3^{2-}$, is also possible at $\text{pH} > 7$ in equilibrium with the atmosphere. Another

study (27) has also suggested that Pu carbonate species could also be dominant at Mayak (fig. S3), although the latest compilation of the thermodynamic database for Pu speciation gives only the maximum possible value for the equilibrium constant of this species because the experimental data are scattered (28). Thus, the carbonate species was not included in the calculations used to produce Fig. 2, B and D. If the Pu is present as a carbonate species in the Mayak system, the negatively charged Pu species can be sorbed by HFO, as could the U carbonate species. Ultimately, the polymerization of carbonate species might result in Pu association with U. Although further analysis is required, we conclude that both Pu and U species are adsorbed similarly onto the HFO surface.

The subsurface migration of Pu from Lake Karachai over more than 4 km within ~55 years after discharge is comparable to the transport rate seen at the Nevada Test Site (1.3 km/30 years minimum) (9). Up until now, there has been an argument over which colloidal phase carries Pu and how they associate. Our evidence of Pu sorption onto the specific colloidal phase is applicable to systems that are dominated by U under oxidizing conditions, such as the proposed repository at Yucca Mountain in Nevada. Because of differences in physicochemical conditions, site-

specific investigations of actinide colloids in the far-field are necessary at each potential nuclear waste repository site.

References and Notes

- J. F. McCarthy, J. M. Zachara, *Environ. Sci. Technol.* **23**, 496 (1989).
- J. I. Kim, *Mater. Res. Soc. Bull.* **19**, 47 (1994).
- J. I. Kim, *Radiochim. Acta* **52/53**, 71 (1991).
- C. Degueldre *et al.*, *Appl. Geochem.* **15**, 1043 (2000).
- J. I. Kim, *Mater. Res. Soc. Symp. Proc.* **294**, 3 (1993).
- W. R. Penrose, W. L. Polzer, E. H. Essington, D. M. Nelson, K. A. Orlandini, *Environ. Sci. Technol.* **24**, 228 (1990).
- R. C. Marty, D. Bennett, P. Thullen, *Environ. Sci. Technol.* **31**, 2020 (1997).
- D. I. Kaplan, P. M. Bertsch, D. C. Adriano, K. A. Orlandini, *Radiochim. Acta* **66/67**, 181 (1994).
- A. B. Kersting *et al.*, *Nature* **396**, 56 (1999).
- J. S. Contardi, D. R. Turner, T. M. Ahn, *J. Contaminant Hydrol.* **47**, 323 (2001).
- W. L. Keeney-Kennicutt, J. W. Morse, *Geochim. Cosmochim. Acta* **49**, 2577 (1985).
- A. L. Sanchez, J. W. Murray, T. H. Sibley, *Geochim. Cosmochim. Acta* **49**, 2297 (1985).
- M. C. Duff *et al.*, *Environ. Sci. Technol.* **33**, 2163 (1999).
- Mayak produced Pu for nuclear weapons by reprocessing spent nuclear fuel. After more than 50 years, there have been major episodes of contamination of the surrounding area—Chelyabinsk, Kurgan, and Sverdlovsk (15, 16).
- B. F. Myasoedov, E. G. Drozko, *J. Alloy. Comp.* **271-273**, 216 (1998).
- G. C. Christensen *et al.*, *Sci. Total Environ.* **202**, 237 (1997).
- N. Solodov, A. V. Zotov, A. D. Khoteev, A. P. Mukhamet-Galeev, B. R. Tagirov, *Appl. Geochem.* **13**, 921 (1998).
- Materials and methods are available as supporting material on Science Online.
- A. P. Novikov *et al.*, "Radiomonitoring of groundwater in the zone of Lake Karachay" (LBNL Report under Contract no. 4698-01-1 p42, Lawrence Berkeley National Laboratory, Berkeley, CA, 1996).
- The Geochemist's Workbench, Release 3.1; RockWare.
- V. Neck, J. I. Kim, *Radiochim. Acta* **89**, 1 (2001).
- G. R. Choppin, *Radiochim. Acta* **91**, 645 (2003).
- M. L. Pierce, C. B. Moore, *Environ. Sci. Technol.* **14**, 214 (1980).
- N. Lu, P. W. Reimus, G. R. Parker, J. L. Conca, I. R. Triay, *Radiochim. Acta* **91**, 713 (2003).
- W. Stumm, J. J. Morgan, *Aquatic Chemistry: An Introduction Emphasizing Chemical Equilibria in Natural Waters* (Wiley-Interscience, New York, ed. 2, 1981), pp. 627–635.
- C. Kantar, B. D. Honeyman, *Radiochim. Acta* **93**, 757 (2005).
- D. L. Clark, D. R. Hobart, M. P. Neu, *Chem. Rev.* **95**, 25 (1995).
- P. Vitorge, H. Capdevila, *Radiochim. Acta* **91**, 623 (2003).
- The work was supported by The Office of Basic Energy Sciences of the U.S. Department of Energy (DE-FG02-04ER15582 and DE-FG03-01ER15168), Russian Academy of Sciences (RCO-20003-SC14 and RGO-20102-RW40), and by Russian Basic Research Foundation (05-03-33028). We thank W. Halsey (Lawrence Livermore National Laboratory) for useful discussion.

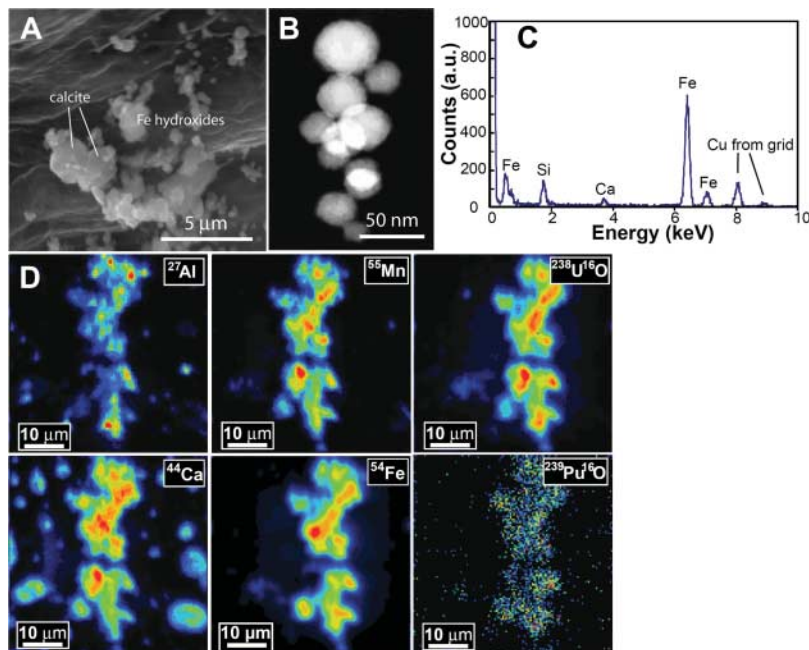


Fig. 3. Direct evidence of Pu adsorption onto amorphous Fe hydroxide. (A) Scanning electron micrograph of typical colloids from well 1/69. Many spherical particles were observed with a size of <1 μm . (B) High-angle annular dark-field scanning transmission electron microscopy image of the spherical colloids. Electron diffraction patterns from these particles indicate that they are amorphous. (C) Energy dispersive x-ray spectrum from the spherical particles shows that Fe is a major constituent associated with trace amounts of Si and Ca. a.u., arbitrary units. (D) Nano-SIMS elemental maps. Because the contrast of these maps has been enhanced to show the distribution clearly, the intensity of the color in the chemical maps corresponds to the relative concentration for each element but cannot be used to compare one element to another.

Supporting Online Material

www.sciencemag.org/cgi/content/full/314/5799/638/DC1
Materials and Methods

Figs. S1 to S3

Table S1

References

15 June 2006; accepted 8 September 2006
10.1126/science.1131307